PAPER

Colloidal synthesis of monodisperse trimetallic Pt-Fe-Ni nanocrystals and their enhanced electrochemical performances

To cite this article: Can Li et al 2023 Nanotechnology 34 075401

View the article online for updates and enhancements.

You may also like

- Ambient Ammonia Electrosynthesis from Nitrogen and Water by Incorporating Palladium in Bimetallic Gold-Silver Nanocages Mohammadreza Nazemi, Luke Soule,

Meilin Liu et al.

- Investigation of Transition Metal-Based (Mn, Co, Ni, Fe) Trimetallic Oxide Nanoparticles on N-doped Carbon Nanotubes as Bifunctional Catalysts for Zn-Air Batteries

Drew Aasen, Michael P. Clark and Douglas G. Ivey

Chemical ordering effect on structural stability of trimetallic Cu-Au-Pt nanoalloys Songül Taran, Ali Kemal Garip and Haydar



Nanotechnology 34 (2023) 075401 (6pp)

https://doi.org/10.1088/1361-6528/aca337

Colloidal synthesis of monodisperse trimetallic Pt–Fe–Ni nanocrystals and their enhanced electrochemical performances

Can Li¹, Jinfong Pan¹, Lihua Zhang^{2,*} and Jiye Fang^{1,*}

E-mail: cli117@binghamton.edu, lhzhang@bnl.gov and jfang@binghamton.edu

Received 11 June 2022, revised 25 October 2022 Accepted for publication 16 November 2022 Published 2 December 2022



Abstract

Among the multi-metallic nanocatalysts, Pt-based alloy nanocrystals (NCs) have demonstrated promising performance in fuel cells and water electrolyzers. Herein, we demonstrate a facile colloidal synthesis of monodisperse trimetallic Pt–Fe–Ni alloy NCs through a co-reduction of metal precursors. The as-synthesized ternary NCs exhibit superior mass and specific activities toward oxygen reduction reaction (ORR), which are \sim 2.8 and 5.6 times as high as those of the benchmark Pt/C catalyst, respectively. The ORR activity of the carbon-supported Pt–Fe–Ni nanocatalyst is persistently retained after the durability test. Owing to the incorporation of Fe and Ni atoms into the Pt lattice, the asprepared trimetallic Pt-alloy electrocatalyst also manifestly enhances the electrochemical activity and durability toward the oxygen evolution reaction with a reduced overpotential when compared with that of the benchmark Pt/C ($\Delta \eta = 0.20$ V, at 10 mA cm⁻²). This synthetic strategy paves the way for improving the reactivity for a broad range of electrocatalytic applications.

Keywords: trimetallic nanocatalyst, ORR, OER

(Some figures may appear in colour only in the online journal)

1. Introduction

The development of advanced electrocatalysts is a significant step toward improving their catalytic performance in electrochemical applications such as fuel cells and water electrolysis [1–3]. Due to the sluggish kinetics of oxygen reduction reaction (ORR) and oxygen evolution reaction (OER), considerable efforts have been made to improve the design of nanocatalysts and facilitate the aforementioned reactions [4–6]. Among the reported electrocatalysts, Pt-based nanocrystals (NCs) are still identified as one class of the most promising candidates [7–9].

To lower the cost and tailor the d-band structure of Pt-based catalysts, breakthroughs in advancing their syntheses have been achieved in three aspects: alloying Pt with 3d

transition metals, tuning the particle morphology and size, and optimizing the surface structure and composition [10–14]. For example, the incorporation of a second or third metal into the Pt lattice to form alloys or intermetallics could result in enhanced catalytic performance due to the ligand, ensemble, and strain effects [1, 3, 5]. Using these strategies, shape-, composition- and surface structure-controlled CuNi@Pt-Cu core@shell nanocatalysts, as a paradigm of the synthesis, were developed using octahedral CuNi NCs [15–17] as the template through a colloidal seed-mediated approach [18]. With strain effects and ligand effects presented in such a structure, the resultant nano-architectures demonstrated superior activity for electrochemical methanol oxidation when compared with the benchmark Pt/C and Pt-Cu/C counterparts [19].

Although the intrinsic catalytic properties could be tuned through the ligand, ensemble, and strain effects, which could originate from a bimetallic system, there are still limited

¹ Department of Chemistry, State University of New York at Binghamton, Binghamton, New York 13902, United States of America

² Center for Functional Nanomaterials, Brookhaven National Laboratory, Upton, New York 11973, United States of America

^{*} Authors to whom any correspondence should be addressed.

studies on trimetallic Pt-based nanocatalysts [18, 20-24]. Wang et al reported trimetallic PtPdCu porous nanocubes and nanodendrites by co-reducing Pt, Pd, and Cu precursors in an aqueous solution [23], demonstrating higher mass activity and longer durability toward an electrochemical methanol oxidation reaction (an anode half-reaction of the fuel cells) than those of the benchmark Pt/C catalyst. However, the more sluggish kinetics of ORR (the cathode reaction of the fuel cells) has become the main roadblock to the development of fuel cell technologies. It is urgent to identify and develop efficient and low-cost electrocatalysts for ORR. A recent report showed that sub-6 nm monodisperse ordered L₁₀-Pt-Ni-Co nanoparticles can efficiently enhance the ORR [22], stimulating the interest in developing other types of Ptbased trimetallic electrocatalysts to facilitate the ORR performance.

Herein, we reported a facile one-pot synthesis of trimetallic Pt–Fe–Ni NCs by co-reducing all the metal precursors together. The composition, structure, and size of the resultant products were characterized by using an inductively coupled plasma-optical emission spectrometer (ICP-OES), high-resolution transmission electron microscopy equipped with energy dispersive X-ray (EDX), and X-ray diffraction (XRD). The electrochemical performance of the carbon-supported Pt–Fe–Ni nanocatalyst was also evaluated toward ORR and OER in alkaline media. The as-prepared nanocatalyst exhibited enhanced ORR and OER activities and durability when compared with the benchmark Pt/C samples, paving the way for designing and synthesizing Pt-based trimetallic nanocatalysts with size control.

2. Experimental section

2.1. Chemicals and materials

Oleylamine (OAm, 70%), oleic acid (OA, 90%), anhydrous acetone (99.5%), anhydrous hexane (98.5%), Nafion[®] 117 solution (5%), benzyl ether (BE, 98%), tungsten hexacarbonyl (W(CO)₆, 97%), potassium hydroxide (KOH, 99.95%), and sodium hydroxide (NaOH, 97%) were purchased from Sigma–Aldrich. Platinum (II) acetylacetonate (Pt(acac)₂, 99.9%), iron (II) chloride tetrahydrate (FeCl₂·4H₂O, 95.0%), and nickel (II) chloride hexahydrate (NiCl₂·6H₂O, 99.8%) were obtained from Alfa–Aesar. Perchloric acid (~70%) was ordered from ACROS. Anhydrous ethanol (200 proof) was received from PHARCO-Aaper. The benchmark Pt/C catalyst (containing 20 wt% Pt with support of Vulcan XC-72R) was purchased from Fuel Cells Store.

2.2. Synthesis of Pt-Fe-Ni nanocrystals

Pt–Fe–Ni trimetallic NCs were prepared using a one-pot colloidal synthetic method. Typically, 0.05 mmol of FeCl₂·4H₂O, 0.05 mmol of NiCl₂·6H₂O, and 0.05 mmol of Pt(acac)₂ were loaded into a three-neck flask containing 7.0 ml of BE, 2.0 ml of OAm, and 1.0 ml of OA. After degassing the mixture under vacuum at 110 °C for at least 1 h,

the clear solution was heated to $130~^{\circ}\text{C}$ in 3 min under the protection of an argon atmosphere. 50.0~mg of $W(\text{CO})_6$ was added to the vigorously stirred solution. The temperature was then raised to $230~^{\circ}\text{C}$ within 10~min and remained there for 30~min before cooling to room temperature. The resultant dark-brown suspensions were precipitated by adding 20~ml of mixed absolute ethanol and hexane (1:1 in vol) and subsequent centrifugation. The precipitates were further dissolved in 10~ml of hexane and re-precipitated by adding 10~ml of absolute ethanol and centrifugation, followed by one more cycle of washing. The cleaned Pt–Fe–Ni nanocatalyst was finally dispersed in anhydrous hexane as stocking suspensions protected using an argon atmosphere.

2.3. Catalyst ink preparation and electrochemical evaluation

To prepare carbon-supported Pt–Fe–Ni nanocatalyst (~20 wt% Pt), a certain amount of the Pt-Fe-Ni stock suspensions in hexane were drop-wisely added to the mixture of hexane/ carbon black (Ketjen black, EC600) with desired carbon fraction under an ultrasonication (the temperature was maintained around 0 °C using an ice-bath). Once this step was complete, the carbon-loaded nanocatalyst was further cleaned using 0.1 M NaOH/CH₃OH solution and collected by centrifugation at 9,000 rpm. They were further washed using ethanol at least three times to remove the potential organic residues. Finally, the carbon-supported nanocatalyst was dried in a vacuum oven at room temperature (~21 °C) overnight to remove the solvent. The actual Pt-fraction in the as-prepared nanocatalyst was determined using ICP-OES, and accordingly adjusted. 4.0 mg of the carbon-loaded nanocatalyst (designated as Pt-Fe-Ni NCs/C, vide infra) were dispersed into 2.0 ml of a pre-prepared solution consisting of 1.6 ml of ultrapure water, 0.4 ml of isopropanol, and 20.0 μ l of Nafion solution (5 wt%), yielding a homogenous ink solution. Next, 20 μ l of such a catalyst ink was deposited onto a glassy carbon (GC) rotating disk electrode (RDE, 5 mm in diameter) and dried naturally to form a uniform thin film for the electrochemical evaluation. The film of benchmark Pt/C (20 wt% Pt) catalyst was prepared on an RDE using the same procedure. The final mass loadings of Pt for Pt-Fe-Ni NCs/C and for benchmark Pt/C on the electrode were determined as 20 μ g cm⁻².

For the ORR study, electrochemical activation of the asprepared nanocatalyst on a GC RDE was performed at an electrochemical workstation (Gamry, 1000E) by 50 cycles of cyclic voltammetry (CV) between 0.05 and 1.2 V versus reversible working electrode (RHE) at a sweeping rate of 100 mV⋅s⁻¹ in N₂-saturated 0.1 M HClO₄ solution. We used acidic media in this step since the existence of oxophilic Ni and/or Fe components on the catalyst surface might block the subsequent ORR performance [25]. ORR polarization curves were then recorded using the linear sweep voltammetry (LSV) technique at a scan rate of 5 mV·s⁻¹ and a rotating rate of 1,600 rpm in O₂-saturated 0.1 M KOH solution. The kinetic current (j_k) at 0.9 V (versus RHE) was derived from the Koutecký–Levich equation: $j_k = (j_{lim} \times j)/(j_{lim} - j)$, where j_{lim} is the kinetically limited current, j is the measured current density. The mass activity (MA, A/mg) was calculated using

the equation: $MA = j_k/m_{Pt}$, where the m_{Pt} stands for the mass of element Pt loaded on the electrode.

For the OER study, electrochemical activation of the asprepared nanocatalyst on a GC RDE was similarly performed by 50 cycles of CV between 0.05 and 1.2 V (*versus* RHE) at a sweeping rate of 100 mV·s⁻¹ in N₂-saturated 1 M KOH solution. OER polarization curves were then recorded using LSV mode in O₂-saturated 1 M KOH solution at a scan rate of 5 mV s⁻¹ in the range of 1.2 V to 2.0 V (*versus* RHE).

A Ag/AgCl electrode in saturated KCl solution and a graphite rod were used as the reference and counter electrodes, respectively. All potentials referred to as the RHE were converted using the equation of $E_{\rm RHE}=E_{\rm Ag/AgCl}+0.059\times {\rm pH}+0.197$. The overpotential (η) of OER was calculated using the following formula: $\eta=E_{\rm RHE}-1.23~{\rm V}$.

2.4. Structure and composition characterizations

A 200 kV field-emission transmission electron microscope (TEM) and a JEOL 2100F TEM were used for collecting low-resolution TEM images. Hitachi 2700C TEM was used for HAADF-STEM imaging as well as EDX elemental mapping. Composition analysis was carried out on an Optima 7000 DV ICP-OES spectrometer. XRD characterization was carried out using a Panalytical X-ray diffractometer equipped with a Cu K αI source, $\lambda = 1.54056$ Å. The diffraction signals were recorded with the 2θ step size of 0.02° .

3. Results and discussion

In the Pt-Fe-Ni NC preparation, we adopted the bimetallic synthesis strategy that we reported previously [26, 27]. The tungsten (W) and gaseous carbon monoxide (CO) in situ released through the thermal decomposition of W(CO)₆ act as a reducing agent and a facet-crystallization facilitator for Ptbased products, respectively. Figure 1(a) shows a typical TEM image of the as-synthesized Pt-Fe-Ni NCs with an average diameter of 8.7 ± 0.5 nm (figure 1(b)). The high-resolution TEM (HRTEM) image taken from an individual NC along the [001] zone axis is shown in figure 1(c). The lattice spacings are measured to be 2.24 Å and 1.94 Å, corresponding to the (111) and (200) planes of the Pt-Fe-Ni NC. These values also match well with the (111) and (200) lattice spacing calculated from the powder XRD pattern shown in figure 1(d). Furthermore, the alloyed Pt-Fe-Ni structure with uniform distributions of Pt, Ni, and Fe is validated by the EDX elemental mapping on a typical NC (figure 2(a)-(c)). HAADF-STEM EDX line scan profile across a typical Pt-Fe-Ni NC shown in figure 2(d) confirmed that all the metal elements are saturated and distributed uniformly across the whole NC. The atomic proportion of Pt, Fe, and Ni in the Pt-Fe-Ni NC was determined as 76: 16:8, which is considered consistent with the molar fraction of Pt, Fe, and Ni determined using ICP-OES (Pt : Fe : Ni = 73 : 17:10).

To evaluate the electrochemical performance, the pristine Pt-Fe-Ni NCs were first loaded onto carbon black as described above, denoted as Pt-Fe-Ni NCs/C. The HAADF-

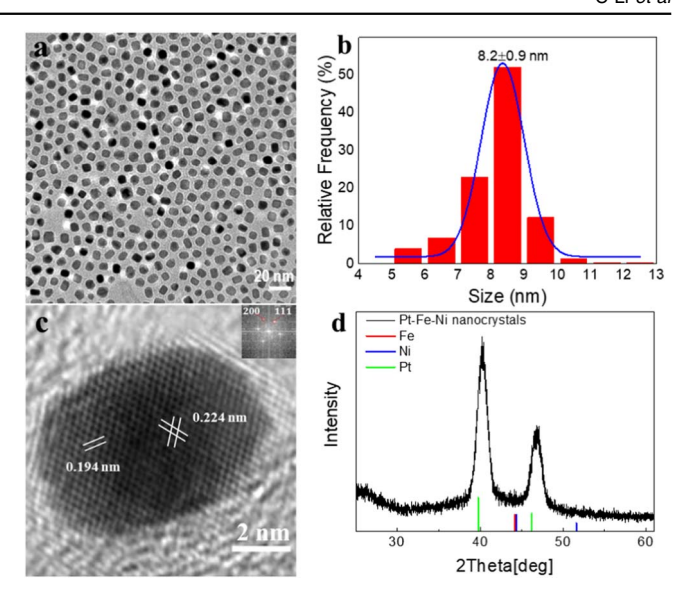


Figure 1. A typical TEM image (a) and the corresponding size distribution histogram (b) of the as-prepared Pt–Fe–Ni NCs. (c) HRTEM image of a typical Pt–Fe–Ni NC. (d) XRD pattern of the carbon-supported Pt–Fe–Ni NCs (Pt–Fe–Ni NCs/C). The lines on the bottom represent standard JCPDS ICDD cards. Green: Pt, 01–1190; blue: Ni, 01–1258; red: Fe, 01–1252.

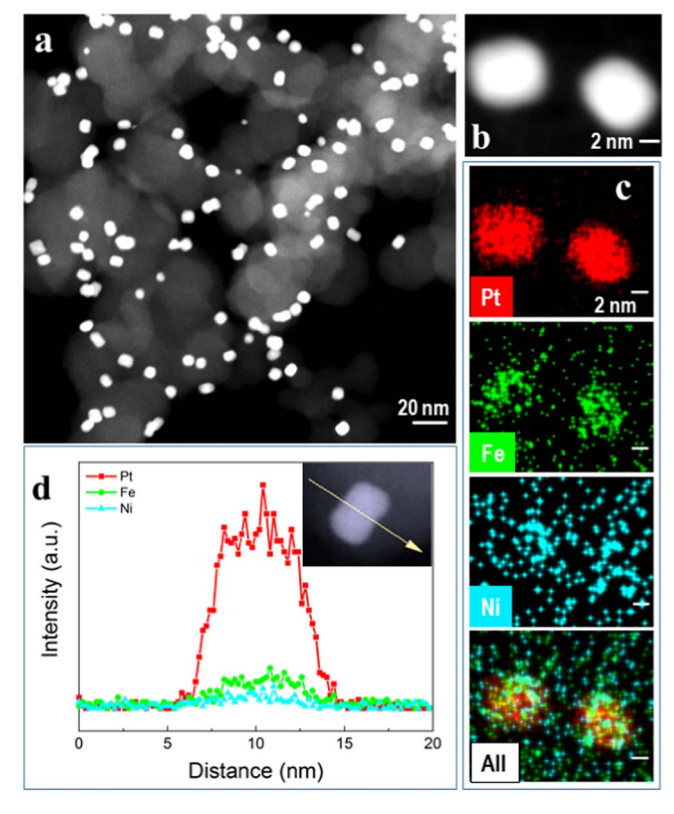


Figure 2. (a, b) HAADF-STEM image of Pt–Fe–Ni NCs/C catalysts, (c) EDX elemental mapping of two individual Pt–Fe–Ni NCs, and (d) HAADF-STEM EDX line scan profile across a typical Pt–Fe–Ni NC.

STEM image of the Pt–Fe–Ni NCs/C nanocatalyst shown in figure 2(a) illustrates a considerably homogenous distribution of NCs on the carbon support. After transferring the catalysts Pt–Fe–Ni NCs/C and benchmark Pt/C onto RDE, their

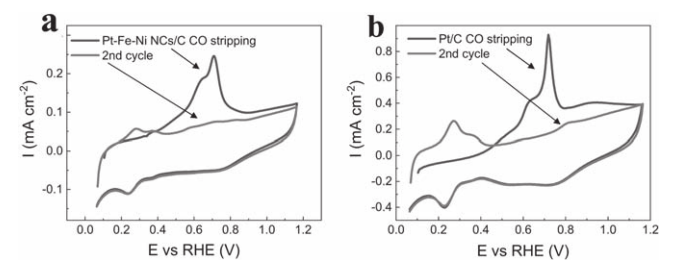


Figure 3. The CO striping and the following cyclic voltammetry curves of Pt–Fe–Ni NCs/C (a) and the benchmark Pt/C (b) in N_2 -saturated 0.1 M KOH solution. Scanning rate: 50 mV s⁻¹.

catalytic activities of ORR and OER were subsequently evaluated in O₂-saturated 0.1 M KOH and 1 M KOH solutions, respectively. Before these determinations, CO-stripping curves and CV profiles were also acquired accordingly.

Figures 3(a), (b) presents the CO-stripping curves (black line) and CV profiles (red line) in the potential range of 0.05-1.2 V versus RHE. To calculate the specific electrochemical surface area (ECSAsH-upd) determined from hydrogen UPD (H_{UPD}), charges from CV curves were integrated with the potential range of 0.1-0.5 V. The specific ECSAs_{H-upd} of Pt-Fe-Ni NCs/C and Pt/C were determined as $29 \text{ m}^2 \text{ g}^{-1}$ and $68 \text{ m}^2 \text{ g}^{-1}$, respectively. The specific ECSAs were further confirmed using a CO-stripping experiment in 0.1 M KOH solution as well (designated as 'ECSAs_{CO}'). As indicated in figure 3, the ECSAs_{CO} of Pt-Fe-Ni NCs/C and Pt/C were determined by integrating charges from CO-striping peaks in the potential range of 0.4-1.0 V, and calculated as $36 \text{ m}^2 \text{ g}^{-1}$ and $72 \text{ m}^2 \text{ g}^{-1}$, respectively. The ratio of ESCAs calculated from the H_{UPD} and CO-stripping for Pt-Fe-Ni NCs/C was 1.00: 1.29. This result is in agreement with the previous observation, in which the H_{UPD} of Pt-based nanoalloys was substantially suppressed when compared to that of pure Pt due to the altered electronic structure on their Pt-skin-like surface [28–31]. In addition, the intensity of a shoulder peak around 0.6 V versus RHE of the CO-stripping profile is stronger in the case of Pt–Fe–Ni NCs/ C than that of the benchmark Pt/C, implying the presence of Fe or Ni atoms on the surface and/or subsurface and the lower CO-stripping potentials facilitated by these 3d-transition atoms [25, 32].

Figure 4(a) shows the positive-going ORR polarization profiles recorded on the Pt–Fe–Ni NCs/C and benchmark Pt/C at a scan rate of 5 mV s⁻¹ and a rotation speed of 1,600 rpm in O₂-saturated 0.1 M KOH solution. Without iR compensation, the Pt–Fe–Ni NCs/C exhibited an $E_{1/2}$ value of 0.890 V versus RHE, which is 25 mV higher than that of Pt/C ($E_{1/2}$ = 0.865 V). Based on the Koutecky–Levich equation with normalization of Pt-mass on the electrode and the ESCAs determined above, the MA and specific activity (SA) were calculated as 0.48 A mg⁻¹ and 1.29 mA cm⁻² (for Pt–Fe–Ni NCs/C), 0.17 A mg⁻¹ and 0.23 mA cm⁻² (for the benchmark Pt/C), respectively. As shown in figures 4(c), (d), the MA and SA Pt–Fe–Ni NCs/C are about ~2.8 times and ~5.6 times as high as those of the benchmark Pt/C. This remarkable improvement could be attributed to the weakening of the

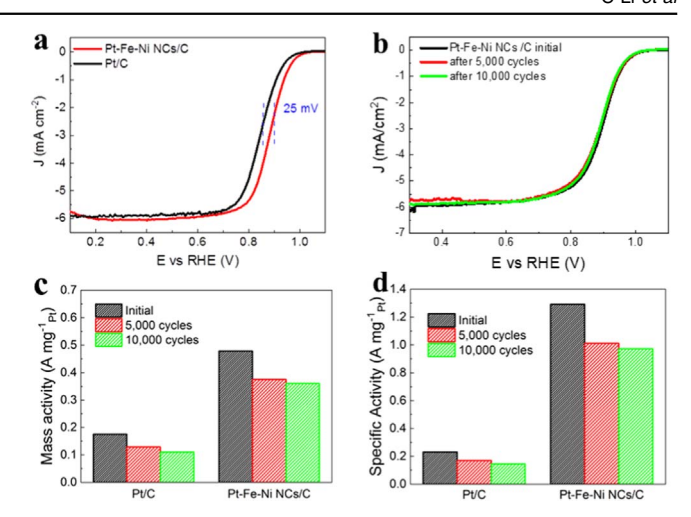


Figure 4. (a) Comparison of positive-going ORR polarization curves between Pt–Fe–Ni NCs/C and the benchmark Pt/C in O₂-saturated 0.1 M KOH solution. (b) Comparison of positive-going ORR polarization curves before and after accelerated durability test of Pt–Fe–Ni NCs/C in O₂-saturated 0.1 M KOH solution. (c) Comparison of Pt mass activity and (d) specific activity of Pt–Fe–Ni NCs/C and the benchmark Pt/C at 0.9 V *versus* RHE. All the ORR polarization curves were obtained at a scan rate of 5 mV s⁻¹ with a rotating speed of 1600 rpm.

adsorption strength between the OH⁻ and the catalytic site due to the downshift of the Pt d-band center arising from the ensemble effect and ligand effect owing to the incorporation of 3d transition metals (Fe and Ni) into the Pt lattice [1, 3]. The modified electronic structure of Pt-Fe-Ni NCs/C facilitates the adsorption of O₂ molecules, promotes the breaking of O-O bond, and boosts the ORR activities. It is worth mentioning that the diffusion-limited current densities of both the Pt-Fe-Ni NCs/C and Pt/C were measured as around -5.8 mA cm^{-2} under the condition of a scan rate of 5 mV s⁻¹ and a rotation rate of 1,600 rpm, showing a four-electron (4e⁻) oxygen reduction mechanism of producing water directly as the determined current densities are consistent with the typical value (~5.7 mA cm⁻²) for the 4e⁻ oxygen reduction in O2-saturated 0.1 M KOH solution according to the Levich equation [33, 34]. The accelerated durability test (ADT) was conducted by applying continuous potential cycling in the range of 0.6-1.0 V versus RHE in the O₂-saturated 0.1 M KOH solution. Figure 4(b) showed the ORR polarization curves recorded from the as-prepared Pt-Fe-Ni NCs/C catalysts, after 5,000 and 10,000 of potential cycles, respectively. A downshift of only 6 mV of $E_{1/2}$ value for the Pt-Fe-Ni NCs/C was observed at the ADT after 10,000 of potential cycles, indicating that the catalyst is considerably stable. Figures 4(c), (d) illustrates the ADTdependent MA and SA of both types of catalysts. The MA and SA of Pt-Fe-Ni NCs/C dropped 23% and 25%, respectively. Compared to the Pt/C which dropped 47% and 40%, respectively, the less degradation of MA and SA for the Pt-Fe-Ni NCs/C indicates their better stability toward ORR in the alkaline media. It is believed that activity decay is mainly due to the particle aggregation based on our TEM

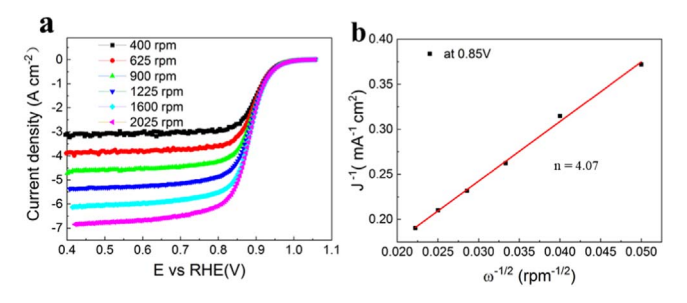


Figure 5. (a) ORR performance of Pt–Fe–Ni NCs/C catalyst in O₂-saturated 0.1 M KOH at a scan rate of 5 mV s⁻¹ and different rotation speeds. (b) The Koutecky–Levich plot (J⁻¹ *versus* $\omega^{-1/2}$) on Pt–Fe–Ni NCs/C catalysts.

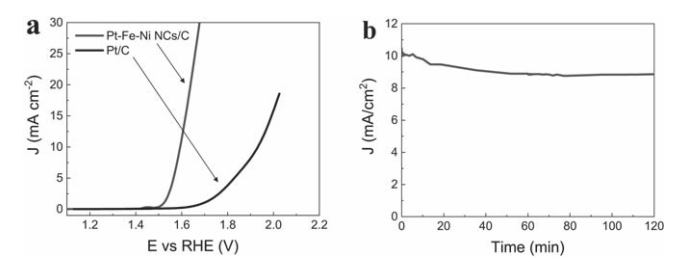


Figure 6. (a) Polarization curves achieved in O_2 -saturated 1 M KOH solution for the Pt–Fe–Ni NCs/C and the benchmark Pt/C catalysts. Scan rate: 5 mV s⁻¹; rotation speed: 1,600 rpm. (b) Time dependence of the current density in O_2 -saturated 1 M KOH solution of the Pt–Fe–Ni NCs/C on a GC RDE with a 1,600 rpm rotating speed.

image evaluation (not shown), rather than the leaching of 3d transition metals which usually happens in acidic media.

Furthermore, the corresponding Koutecky–Levich (K–L) plot (j^{-1} versus $\omega^{-1/2}$) derived from the RDE voltammograms (figure 5(a)) at 0.85 V is presented in figure 5(b). The K–L plot displays good linearity and parallelism for the Pt–Fe–Ni NCs /C catalysts, revealing the first-order reaction kinetics for ORR as a function of the concentration of dissolved oxygen. Using the K–L equation, the electron transfer number (n) was then calculated as 4.07, supporting the hypothesis of a 4e $^-$ oxygen reduction mechanism on the Pt–Fe–Ni NCs /C.

Figure 6(a) shows the polarization curves of the Pt-Fe-Ni NCs/C and Pt/C toward OER at a scan rate of 10 mV s⁻¹ and a rotating speed of 1,600 rpm in O₂-saturated 1 M KOH solution. The Pt-Fe-Ni NCs/C achieves 10 mA cm⁻² current density at an overpotential of $\eta = 0.40 \pm 0.05$ V, whereas the benchmark Pt/C gives an overpotential of 0.61 \pm 0.05 V. It is apparent that the former required much lower overpotential when compared with the latter ($\triangle \eta = 0.20 \text{ V}$), indicating its superior OER activity. Yu et al reported Ni-Fe layered double hydroxide hollow nanoprisms with large surface areas as well as the Ni-Fe synergistic effect, manifesting high electrocatalytic activity toward the OER with low overpotential and remarkable stability [35]. We consequently believe that optimization in the composition and specific surface area could result in further improvement. We also propose that the presence of Ni and Fe on the surface of Pt-Fe-Ni NCs plays the role of decreasing the oxidation energy barrier by controlling the active catalytic sites [36, 37]. The long-term durability of Pt–Fe–Ni NCs/C catalyst was tested by a chronopotentiometry (CP) measurement on GC at $\eta=0.40$ V (figure 6(b)). The current density, j, generally remained stable over 2 h with acceptable degradation (\sim 11%). Based on these evaluation results, we conclude that the Pt–Fe–Ni NCs/C outperform the benchmark Pt/C in their OER performance.

4. Conclusions

We report a facile colloidal synthesis approach for the preparation of monodisperse Pt-Fe-Ni NCs. The produced trimetallic nanocatalyst, Pt-Fe-Ni NCs/C, exhibited superior mass and specific activities toward ORR in alkaline media, showing \sim 2.8- and 5.6-times as high as those of benchmark Pt/C catalyst, respectively. An ADT indicated that the activity of Pt-Fe-Ni NCs/C was considerably retained after 10,000 of potential cycles in 0.1 M KOH solution. Due to the incorporation of Fe and Ni atoms in Pt-lattice, this trimetallic electrocatalyst also manifests enhanced electrochemical performance toward OER with a smaller overpotential when compared with the Pt/C ($\Delta \eta = 0.20 \text{ V}$). Taken together, this work not only showcases the feasibility of the Pt-based trimetallic NC synthesis but also demonstrates the effect of ORR and OER enhancement in alkaline media when 3d transition elements are introduced into the Pt lattice.

Acknowledgments

This work was primarily supported by the National Science Foundation under Grant # DMR 1808383. CL and JP were also partially supported by the Center for Alkaline-Based Energy Solutions (CABES), an Energy Frontier Research Center funded by the U.S. Department of Energy, Office of Science, Basic Energy Sciences under award # DE-SC0019445. LZ acknowledges the use of TEM facilities for the structural characterizations, at the Center for Functional Nanomaterials, Brookhaven National Laboratory, which is supported by the U.S. DOE, Office of Science, Basic Energy Sciences under Contract No. DE-SC0012704. Partial low-magnification TEM imaging work was supported by S3IP/ADL, the State University of New York at Binghamton. We also appreciate the Harpur College Faculty Research Grant/Subvention Fund for supporting the color figure print.

Data availability statement

The data that support the findings of this study are available upon reasonable request from the authors.

ORCID iDs

Can Li https://orcid.org/0000-0001-8894-5110
Lihua Zhang https://orcid.org/0000-0003-3331-2345
Jiye Fang https://orcid.org/0000-0003-3703-3204

References

- [1] Li C, Yan S and Fang J 2021 Construction of lattice strain in bimetallic nanostructures and its effectiveness in electrochemical applications *Small* 17 2102244
- [2] Xie Y, Li C, Razek S A, Fang J and Dimitrov N 2020 Synthesis of nanoporous Au-Cu-Pt alloy as a superior catalyst for the methanol oxidation reaction ChemElectroChem 7 569–80
- [3] Zhou M, Li C and Fang J 2021 Noble-metal based random alloy and intermetallic nanocrystals: syntheses and applications *Chem. Rev.* 121 736–95
- [4] Gewirth A A, Varnell J A and DiAscro A M 2018 Nonprecious metal catalysts for oxygen reduction in heterogeneous aqueous systems *Chem. Rev.* 118 2313–39
- [5] Gilroy K D, Ruditskiy A, Peng H-C, Qin D and Xia Y 2016 Bimetallic nanocrystals: syntheses, properties, and applications *Chem. Rev.* 116 10414–72
- [6] Kulkarni A, Siahrostami S, Patel A and Nørskov J K 2018 Understanding catalytic activity trends in the oxygen reduction reaction *Chem. Rev.* 118 2302–12
- [7] Kong F et al 2020 Active and stable Pt-Ni alloy octahedra catalyst for oxygen reduction via near-surface atomical engineering ACS Catal. 10 4205-14
- [8] Xie M, Lyu Z, Chen R, Shen M, Cao Z and Xia Y 2021 Pt-Co@Pt octahedral nanocrystals: enhancing their activity and durability toward oxygen reduction with an intermetallic core and an ultrathin shell J. Am. Chem. Soc. 143 8509–18
- [9] Ze H, Chen X, Wang X-T, Wang Y-H, Chen Q-Q, Lin J-S, Zhang Y-J, Zhang X-G, Tian Z-Q and Li J-F 2021 Molecular insight of the critical role of Ni in Pt-based nanocatalysts for improving the oxygen reduction reaction probed using an *in situ* SERS borrowing strategy *J. Am. Chem. Soc.* 143 1318–22
- [10] Liu J and Zhang J 2020 Nanointerface chemistry: lattice-mismatch-directed synthesis and application of hybrid nanocrystals *Chem. Rev.* 120 2123–70
- [11] He T, Wang W, Shi F, Yang X, Li X, Wu J, Yin Y and Jin M 2021 Mastering the surface strain of platinum catalysts for efficient electrocatalysis *Nature* 598 76–81
- [12] Kim C, Dionigi F, Beermann V, Wang X, Moller T and Strasser P 2019 Alloy nanocatalysts for the electrochemical oxygen reduction (ORR) and the direct electrochemical carbon dioxide reduction reaction (CO₂ RR) Adv. Mater. 31 1805617
- [13] Quan Z, Wang Y and Fang J 2013 High-index faceted noble metal nanocrystals Acc. Chem. Res. 46 191–202
- [14] Porter N S, Wu H, Quan Z and Fang J 2013 Shape-control and electrocatalytic activity-enhancement of Pt-based bimetallic nanocrystals Acc. Chem. Res. 46 1867–77
- [15] Li C, Luan Y, Zhao B, Kumbhar A, Chen X, Collins D, Zhou G and Fang J 2020 Facet-dependent catalysis of CuNi nanocatalysts toward 4-nitrophenol reduction reaction MRS Adv. 5 1491-6
- [16] Li C, Luan Y, Zhao B, Kumbhar A and Fang J 2019 Size-controlled synthesis of CuNi nano-octahedra and their catalytic performance towards 4-nitrophenol reduction reaction MRS Adv. 4 263–9
- [17] Wang M, Wang L, Li H, Du W, Khan M U, Zhao S, Ma C, Li Z and Zeng J 2015 Ratio-controlled synthesis of CuNi octahedra and nanocubes with enhanced catalytic activity J. Am. Chem. Soc. 137 14027–30
- [18] Li C, Chen X, Zhang L, Yan S, Sharma A, Zhao B, Kumbhar A, Zhou G and Fang J 2021 Synthesis of core@shell Cu-Ni@Pt-Cu nano-octahedra and their improved MOR activity Angew. Chem. Int. Ed. 60 7675–80
- [19] Xu D, Liu Z, Yang H, Liu Q, Zhang J, Fang J, Zou S and Sun K 2009 Solution-based evolution and enhanced

- methanol oxidation activity of monodisperse platinum-copper nanocubes *Angew*. *Chem. Int. Ed.* **48** 4217–21
- [20] Qin Y et al 2020 Fine-tuning intrinsic strain in penta-twinned Pt-Cu-Mn nanoframes boosts oxygen reduction catalysis Adv. Funct. Mater. 30 1910107
- [21] Li H et al 2020 Surface oxygen-mediated ultrathin PtRuM (Ni, Fe, and Co) nanowires boosting methanol oxidation reaction J. Mater. Chem. A 8 2323–30
- [22] Wang T et al 2019 Sub-6 nm fully ordered L1₀-Pt-Ni-Co nanoparticles enhance oxygen reduction via Co doping induced ferromagnetism enhancement and optimized surface strain Adv. Energy Mater. 9 1803771
- [23] Wang P, Zhang Y, Shi R and Wang Z 2019 Shape-controlled synthesis of trimetallic PtPdCu nanocrystals and their electrocatalytic properties ACS Appl. Energy Mater. 2 2515–23
- [24] Zhang S, Hao Y, Su D, Doan-Nguyen V V T, Wu Y, Li J, Sun S and Murray C B 2014 Monodisperse core/shell Ni/ FePt nanoparticles and their conversion to Ni/Pt to catalyze oxygen reduction J. Am. Chem. Soc. 136 15921–4
- [25] Rudi S, Teschner D, Beermann V, Hetaba W, Gan L, Cui C, Gliech M, Schlögl R and Strasser P 2017 pH-Induced versus oxygen-induced surface enrichment and segregation effects in Pt–Ni alloy nanoparticle fuel cell catalysts ACS Catal. 7 6376–84
- [26] Zhang J and Fang J 2009 A general strategy for preparation of Pt 3d-transition metal (Co, Fe, Ni) nanocubes J. Am. Chem. Soc. 131 18543–7
- [27] Zhang J, Yang H, Fang J and Zou S 2010 Synthesis and oxygen reduction activity of shape-controlled Pt₃Ni nanopolyhedra *Nano Lett.* 10 638–44
- [28] Shao M, Odell J H, Choi S-I and Xia Y 2013 Electrochemical surface area measurements of platinum- and palladiumbased nanoparticles *Electrochem. Commun.* 31 46–8
- [29] Choi S-I et al 2013 Synthesis and characterization of 9 nm Pt-Ni octahedra with a record high activity of 3.3 A/mgPt for the oxygen reduction reaction Nano Lett. 13 3420-5
- [30] van der Vliet D F, Wang C, Li D, Paulikas A P, Greeley J, Rankin R B, Strmenik D, Tripkovic D, Markovic N M and Stamenkovic V R 2012 Unique electrochemical adsorption properties of Pt-skin surfaces Angew. Chem. Int. Ed. 124 3193–6
- [31] Stamenkovic V R, Fowler B, Mun B S, Wang G, Ross P N, Lucas C A and Marković N M 2007 Improved oxygen reduction activity on Pt₃Ni(111) via increased surface site availability Science 315 493–7
- [32] Huang W et al 2015 Highly active and durable methanol oxidation electrocatalyst based on the synergy of platinumnickel hydroxide-graphene Nat. Commun. 6 10035
- [33] Ge Y *et al* 2021 Seeded synthesis of unconventional 2H-phase Pd alloy nanomaterials for highly efficient oxygen reduction *J. Am. Chem. Soc.* **143** 17292–9
- [34] Zhou M, Guo J, Zhao B, Li C, Zhang L and Fang J 2021 Improvement of oxygen reduction performance in alkaline media by tuning phase structure of Pd–Bi nanocatalysts J. Am. Chem. Soc. 143 15891–7
- [35] Yu L, Yang J F, Guan B Y, Lu Y and Lou X W 2018 Hierarchical hollow nanoprisms based on ultrathin Ni–Fe layered double hydroxide nanosheets with enhanced electrocatalytic activity towards oxygen evolution *Angew*. *Chem. Int. Ed.* 57 172–6
- [36] Yu L, Yang J F, Guan B Y, Lu Y and Lou X W 2018 Hierarchical hollow nanoprisms based on ultrathin Ni–Fe layered double hydroxide nanosheets with enhanced electrocatalytic activity towards oxygen evolution *Angew*. Chem. Int. Ed. 57 172–6
- [37] Strickler A L, Escudero-Escribano M A and Jaramillo T F 2017 Core-shell Au@metal-oxide nanoparticle electrocatalysts for enhanced oxygen evolution *Nano Lett.* 17 6040–6